Available online at www.sciencedirect.com
ScienceDirect
Journal of Computational Physics 227 (2008) 5385–5396
JOURNAL OF COMPUTATIONAL PHYSICS
www.elsevier.com/locate/jcp

Verification of a fluid-dynamics solver using correlations with linear stability results

G. Matheou [a,*], C. Pantano [b], P.E. Dimotakis [a]

[a] Graduate Aeronautical Laboratories, California Institute of Technology, Pasadena, CA 91125, USA
[b] Department of Mechanical Science and Engineering, University of Illinois at Urbana-Champaign, Urbana, IL 61801, USA

Received 4 November 2006; received in revised form 12 January 2008; accepted 25 January 2008
Available online 12 February 2008

Abstract

A novel method is described for verification of fluid-dynamics solvers based on correlations with solutions from linear stability analysis. A difficulty with the linear stability analysis solutions for spatially developing flows is that flow fields typically exhibit exponentially growing features compromising the performance of classical error metrics. This motivates the construction of a projection-based metric that only assumes the shape of the solution and not the growth rate of the perturbations, thus also allowing the latter to be determined. The proposed correlation metric complements classical error metrics, such as p-norms, and can also be used for time-dependent problems with realistic boundary conditions. We demonstrate how the present method can be applied in the verification of an Euler solver for the instability behavior of laminar compressible free and confined shear layers.

Keywords: Verification; Linear stability analysis; Correlation; Projection; Shear layer

1. Introduction

Verification techniques in computational fluid dynamics can rely on grid convergence, order of accuracy, Richardson extrapolation, and comparison to benchmark solutions. Numerical results can also be compared against known analytical solutions or against fictitious manufactured solutions [13,28]. A number of reviews have compiled these and other techniques to assess program code accuracy [13,19,26,27]. The challenge of verifying a code with tens or hundreds of thousands of lines in which multi-physics models are involved is considerable [9]. Moreover, although it is theoretically possible to perform many such studies, they are rarely performed without altering some, perhaps substantial, parts of the code. The additional code then renders the original code verification subject to uncertainty. Considerable effort is typically required to implement a thorough verification, despite which one can never be completely certain that all programming or other errors have been uncovered and corrected.

* Corresponding author.
E-mail address: matheou@tyrvos.caltech.edu (G. Matheou).

0021-9991/$ - see front matter © 2008 Elsevier Inc. All rights reserved.
doi:10.1016/j.jcp.2008.01.055

In the work presented here, of concern is how the metric is constructed, since results generally depend on the error norm used to obtain the metric. In classical numerical-analysis terms, an error infinity-, 1-, or 2-norm is used to measure the rate of convergence of the numerical solution and to compare it with the expected value according to the discretization method. While these norms are equivalent for a fixed number of variables and size of the discretization space, they may report different rates of convergence, in practice. This does not invalidate the equivalence of the norms since the size of the discretization space is not fixed when resolution is increased to establish the rate of convergence of the solution. This difficulty also affects the method of manufactured solutions, unless the underlying mathematical problem is rather simple. Moreover, the characteristics of the base or reference solution, against which one compares the computational result, can induce misleading measurements. For example, consider a feature of the analytical or exact solution that is orders of magnitude larger than typical values in most of the domain. The numerical error reported by standard metrics tends to be primarily controlled by errors occurring around the dominant feature. Even when locally scaled metrics are used, there is always a trade-off between how local the scaling can be made and how meaningful the metric results are. If the solution is smooth or monotone, an appropriately scaled error metric may be sufficient. Unfortunately, this is rarely the case with spatially developing unsteady flows. One could assume that such "spiky" fields are rather uncommon. However, most unstable flows behave in this manner, exhibiting an exponentially growing solution in space or time that is, initially, of small amplitude.

As a complement to traditional error metrics one can exploit statistical tools. That is, instead of attempting to obtain a hard measurement of the numerical error, one can attempt to determine how close the numerical solution is to the expected prediction. We note that the value of this metric can be lower than that provided by convergence and accuracy tests since a solution that appears to be approaching an exact solution may ultimately not even be a mathematically consistent one. The closeness of the solutions can be measured in a number of ways, through projection techniques [24] to two-point correlations [7,16]. For the purpose of verification, correlations can be used in a manner akin to that of identification techniques in image processing where geometrical shapes are identified by correlating an image against all possible sizes, orientations and positions of the corresponding primitive [22].

In this paper, we investigate and assess the use of correlations for verification of fluid-dynamics solvers using linear stability analytical results. The methodology will be illustrated using a compressible shear layer as an example. Previous comparisons of numerical codes with results from linear stability analysis (LSA) can be found in [3,12,25]. In these studies, growth is temporal and only in [3] is a comparison with a Navier–Stokes solver that includes the non-linear terms made. In the present study, the growth of the perturbations is spatial and the comparison is with a fully non-linear Euler solver.

2. Verification statement and metric

For unsteady, spatially evolving fields, common error metrics can perform poorly in cases where some feature is growing very rapidly in one, or more, spatial dimensions. In the case of a laminar, spatially developing shear layer, when forcing with an unstable mode is applied at the inflow, perturbations convect downstream and grow exponentially. This exponential growth of the perturbations produces a spatial field with exponentially large and small features. Linear stability analysis can predict the most-amplified mode and provide a solution to the linearized equations. The goal here is to use this result as part of the verification process of an unsteady fluid-dynamics solver. Because of the spatial character of the flow, the proposed verification is not only of the solver itself, but, in large measure, also a verification of the boundary closure numerical implementation. Time-dependent perturbations are introduced at the inflow and must exit at the outflow in such a way that any spurious reflections at the downstream boundary do not contaminate the flow excessively.

Direct comparison of the numerically computed solution at a given time with the LSA result presents many challenges. Even if the initial perturbation is sufficiently small and the linear approximation holds in the entire computational domain, comparison using classical error norms between two fields that grow exponentially is difficult. Consider, for example, a field that grows exponentially with the x coordinate. A small relative error at large x will be responsible for a much larger contribution to an error metric than an incorrect feature at small x. Moreover, as perturbations grow, non-linearities increase and an accumulation of the global error in such regions may be unavoidable. If the field under consideration is relatively simple, locally scaled error measures

can be constructed. In reality, fluid-dynamic solutions are more complex and construction of such locally scaled error metrics can be difficult and problem-specific.

The key objective of this work is to explore a methodology that does not require extensive knowledge of the mathematical form of the exact non-linear solution, but instead, uses a simplified (LSA) solution that produces meaningful and useful estimates.

LSA yields exact solutions to the linearized equations, subject to certain approximations. Among the most restrictive is that, typically, the basic flow field is assumed to be parallel. By comparing the two solutions using a correlation metric, one would like to confirm that perturbations injected into the flow are computed to grow at the expected rate. This can differ from a comparison in terms of a norm of the error between the LSA field and the computed one owing to the aforementioned dependence on the assumed basic flow.

2.1. Linear stability solution

The stability of laminar shear flows has been considered in many studies. Michalke [18] studied the stability of the temporally growing shear layer with a hyperbolic tangent profile, Lessen et al. [14,15] considered compressible temporal shear layers under the assumption that the flow is iso-energetic (the total enthalpy is constant), while Blumen and Drazin et al. [1,2,6] assumed that the thermodynamic state of the flow is constant. Discussion of a secondary instability in three-dimensional shear layers appearing as streamwise counter-rotating vortices can be found in [17]. In this work, the LSA solution for inviscid compressible free and confined spatial shear layers by Zhuang et al. [31,32] is utilized. Their method for deriving the stability characteristics for compressible spatial shear layers is summarized here. The reader is referred to [31,32] for details.

Consider a two-dimensional flow of two parallel steams. All quantities can be written as a basic profile $\overline{Q}(y)$ plus a perturbation

$$Q(x,y,t) = \overline{Q}(y) + Q'(x,y,t). \tag{1}$$

Disturbance quantities denoted by primes can be written as an eigenmode expansion,

$$Q' = f(y)\exp[\mathrm{i}(\alpha x - \omega t)]. \tag{2}$$

For spatially growing fluctuations, like the ones considered here, ω is a real frequency and $\alpha = \alpha_r + \mathrm{i}\alpha_i$ a complex wave number. The corresponding complex wave velocity can then be written as $c = \omega/\alpha$.

Substituting the expressions for the disturbance quantities into the compressible Euler equations and neglecting quadratic and higher-order terms yields a system of ordinary differential equations for the amplitude functions. These equations can be reduced to a single equation for the pressure disturbances.

For a given disturbance frequency, ω, and a basic flow, the solution of the boundary-value problem for the pressure eigenfunction gives the complex eigenvalue, α. The eigenfunctions for the velocity and density can then be expressed as functions of the pressure eigenfunction and its derivatives and the complete two-dimensional field can then be constructed.

A shooting Runge–Kutta–Fehberg method is used to solve the eigenvalue problem by matching the asymptotic boundary conditions away from the shear layer. Even though analytical solutions are generally preferred for verification, numerical solution methods of ordinary differential equations are well developed and solution techniques are reliable. The numerical solutions of the eigenfunctions are obtained independently of the code being verified, with a typical error of $O(10^{-6})$.

2.2. Metric

We define the correlation r, between the computed perturbation field u'_{comp} and the corresponding field from the LSA, u'_{LSA}, by

$$r = \frac{\langle u'_{\mathrm{comp}} u'_{\mathrm{LSA}} \rangle}{\langle u'^2_{\mathrm{comp}} \rangle^{1/2} \langle u'^2_{\mathrm{LSA}} \rangle^{1/2}}, \tag{3}$$

where

$$\langle\cdot\rangle = \int_V \cdot \, \mathrm{d}\mathbf{x}. \tag{4}$$

The LSA perturbation field is

$$f(y)\mathrm{e}^{-\alpha_\mathrm{i}x+\mathrm{i}\alpha_\mathrm{r}(x-x_0)}, \tag{5}$$

where the eigenfunction f is a function of the vertical coordinate y and also depends implicitly on the mode α, with x_0 a phase shift that will be treated as an independent variable. If a numerical code is correct and the flow is perturbed with the most amplified mode, the correlation r will have a maximum at the value of the most amplified mode.

This correlation may be computed in two different ways. One may assume that near the most amplified mode the shape of the eigenfunction f does not change significantly and neglect the dependence on α. In this case, r is computed for all values of the three-dimensional parameter space $\alpha_\mathrm{r}, \alpha_\mathrm{i}$, and x_0, i.e.,

$$r_1(\alpha_\mathrm{r}, \alpha_\mathrm{i}, x_0) = \frac{\langle u' f(y)\mathrm{e}^{-\alpha_\mathrm{i}x+\mathrm{i}\alpha_\mathrm{r}(x-x_0)}\rangle}{\langle u'^2\rangle^{1/2}\langle (f(y)\mathrm{e}^{-\alpha_\mathrm{i}x+\mathrm{i}\alpha_\mathrm{r}(x-x_0)})^2\rangle^{1/2}}. \tag{6}$$

An alternative is to keep the dependence of the eigenfunction f on the mode α and compute r for values of α along the dispersion relation. In this case, the value of x_0 can be left as a free parameter that can be varied, i.e.,

$$r_2(\alpha(\omega), x_0) = \frac{\langle u' f(\alpha; y)\mathrm{e}^{-\alpha_\mathrm{i}x+\mathrm{i}\alpha_\mathrm{r}(x-x_0)}\rangle}{\langle u'^2\rangle^{1/2}\langle (f(\alpha; y)\mathrm{e}^{-\alpha_\mathrm{i}x+\mathrm{i}\alpha_\mathrm{r}(x-x_0)})^2\rangle^{1/2}}. \tag{7}$$

3. Numerical method

The flow solver assessed here exists at the bottom of an adaptive mesh refinement (AMR) controller called AMROC [4,5] that provides a generic infrastructure for hyperbolic problems and handles mesh adaptation, message passing in parallel architectures, and most of the IO functionality in a quasi-transparent manner. In this study, the AMR capability was not employed and only the two-dimensional version of the solver was used. Thus, a regular Cartesian mesh is used for discretization of the flow fields. The compressible Euler equations were solved with a second-order accurate collocated center-difference scheme discussed in [10]. The method is formulated in energy-conserving form [11], with stable boundary closures [29]. Inflow and outflow boundary conditions are implemented in characteristic form [30,23]. In the present study, the flow field downstream of the outflow boundary can be determined from the LSA, thus the LSA solution is used to obtain the amplitude variation of the incoming wave at the outflow plane. Further details of the complete solver can be found in [20].

4. Results

4.1. Flow description

The shear layer is assumed to be formed between two parallel streams of the same gas governed by the perfect-gas equation of state and subjected to a two-dimensional, spatially growing disturbance. We assume a hyperbolic-tangent basic velocity profile of the form,

$$\overline{U}(y)/U_1 = \eta(y) + U_\mathrm{R}(1-\eta(y)), \tag{8}$$

where $U_\mathrm{R} = U_2/U_1$ is the velocity ratio of the two streams, and

$$\eta(y) = \frac{1}{2}(1+\tanh(y)). \tag{9}$$

As in [31,32], the Crocco–Busemann relation is used to obtain the temperature profile.

The most-amplified mode and the corresponding eigenfunctions are computed from the LSA and used to force the shear layer at the inflow. For example, the streamwise velocity inflow condition is:

$$u(0,y,t) = \overline{U}(y) + \mathcal{A}(f_r(y)\cos(\omega t) - f_i(y)\sin(\omega t)), \tag{10}$$

where f is the complex streamwise velocity eigenfunction, $f = f_r + \mathrm{i}f_i$, and $\mathcal{A}$ is the forcing amplitude. For the present study, the eigenfunctions were normalized such that the maximum of the absolute value of the real part of the streamwise velocity eigenfunction is unity,

$$\max_y(|f_r(y)|) = 1. \tag{11}$$

Two-dimensional numerical simulations of two shear layers were conducted to demonstrate the use of correlations for verification purposes. Shear Layer A is low-Mach-number flow, with a convective Mach number [21] of $M_c = 0.09$. For shear layers composed of the same gas with matched static free-stream pressures and temperatures, the convective Mach numbers, M_{c1} and M_{c2}, are the same from both streams and equal to

$$M_c = \frac{(U_1 - U_2)/2}{a}, \tag{12}$$

where a is the common speed of sound of the two free streams. Shear Layer B has a supersonic top stream over a subsonic stream with $M_c = 0.8$. Shear Layer A is unconfined whereas Shear Layer B is confined. Table 1 summarizes the conditions for the two cases.

The computational domain has a streamwise length of 100 units and a transverse length of 40 units. The shear layer basic profiles are given by Eq. (8). Both cases are computed at four different resolutions to investigate convergence and the effect of grid spacing on the growth rate of the perturbation. Correlations and error metrics are computed up to a streamwise distance of $x = 80$, excluding thereby the region near the outflow boundary.

The computations are initialized with the LSA solution at time $t = 0$ and then the forcing is applied as an inflow perturbation. The amplitude of the forcing ($\mathcal{A}$ in Eq. (10)) is $\mathcal{A} = 0.5 \times 10^{-4} U_1$ for both test cases. Fig. 1 shows a comparison between the computed and the LSA streamwise velocity perturbation fields for Case A.

For the comparison with LSA to be valid, perturbations must be sufficiently small such that the non-linear terms are much smaller that the linear, or first-order terms throughout the domain. The validity of this assumption for the Euler equations is assessed by expressing the system of equations in terms of the primitive-variables vector of state

$$\mathbf{q} = [\,\rho \quad u \quad v \quad T\,]^{\mathrm{T}} \tag{13}$$

as

$$\mathcal{M}(\mathbf{q}) = \mathcal{M}(\bar{\mathbf{q}}) + \mathcal{L}(\mathbf{q}') + \mathcal{N}(\mathbf{q}'), \tag{14}$$

where the terms linear in $\mathbf{q}'$, are in $\mathcal{L}(\mathbf{q}')$ and quadratic and higher-order terms in $\mathcal{N}(\mathbf{q}')$. The linearized equations are a valid approximation to the original set of equations if,

$$\|\mathcal{L}(\mathbf{q}')\| \gg \|\mathcal{N}(\mathbf{q}')\|. \tag{15}$$

Table 1
Flow conditions for the two shear layers

Case	A	B
Transverse boundary	Unconfined	Confined
Top stream Mach number, M_1	0.2	2.133
Convective Mach number, M_c	0.09	0.8
Velocity ratio, U_2/U_1	0.5	0.25
Density ratio, ρ_2/ρ_1	1	1
Temperature ratio, T_2/T_1	1	1

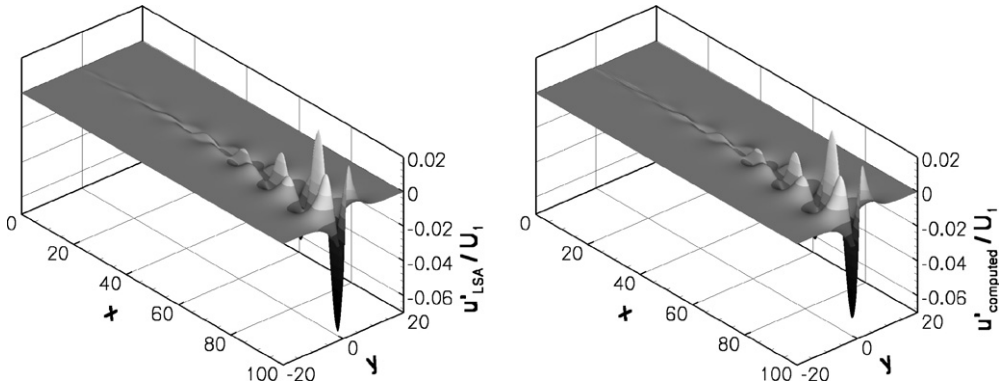

Fig. 1. Streamwise velocity perturbation fields. The panel on the left depicts the linear stability analysis prediction and the one on the right the computed field for Case A, $\Delta x = 0.0625$ and $t = 20$. Note the exponential growth of the perturbation.

For example, for the mass-conservation equation, we must have

$$\left(\int |\mathcal{L}(\rho')|^2 \mathrm{d}\mathbf{x} \right)^{1/2} \gg \left(\int |\mathcal{N}(\rho')|^2 \mathrm{d}\mathbf{x} \right)^{1/2}. \tag{16}$$

The analytical LSA solution was used to compute the norms of the linear and non-linear contributions. Tables 2 and 3 show the results using the L_2 norm. The contribution of the non-linear terms in the momentum equations is always at least two orders of magnitude less than the linear terms. For both test cases, we will accept this as the proper metric for the validity of the linear approximation and that the LSA solution can be compared with the computed fields.

4.2. Classical error metrics

Classical error metrics were computed based on the L_∞ norm. Fig. 2 shows the error norms of the streamwise and transverse velocity perturbations at scaled time, $t = 20$. All times reported are normalized by the mean convective time, $t_c = L_x/U_c$, where L_x is the streamwise length of the computational domain and $U_c = (U_1 + U_2)/2$. The behavior of the error norms is substantially different in the two cases. For Shear Layer B, the error converges at the expected second-order rate. Unlike Case B, the error for Shear Layer A decreases rapidly at coarse resolution but tends to a constant for the finer grids. Two different kinds of error appear to dominate at low and high resolution. At large grid spacings, dispersion errors dominate, but as the grid

Table 2
L_2 norms of the linear and non-linear terms for the unconfined, (effectively) incompressible Shear Layer A

Equation	Linear	Non-linear	Ratio
Mass	1.41×10^{-1}	2.67×10^{-4}	522
x-momentum	$4.00 \times 10^{+1}$	5.50×10^{-3}	7300
y-momentum	$6.98 \times 10^{+1}$	3.28×10^{-3}	21,265
Energy	5.62×10^{-1}	6.02×10^{-2}	9

Table 3
L_2 norms of the linear and non-linear terms for confined, compressible Shear Layer B

Equation	Linear	Non-linear	Ratio
Mass	1.40×10^{-2}	2.60×10^{-7}	53,838
x-momentum	4.17×10^{-1}	3.31×10^{-5}	12,604
y-momentum	1.26	1.85×10^{-5}	68,184
Energy	1.78	8.37×10^{-3}	212

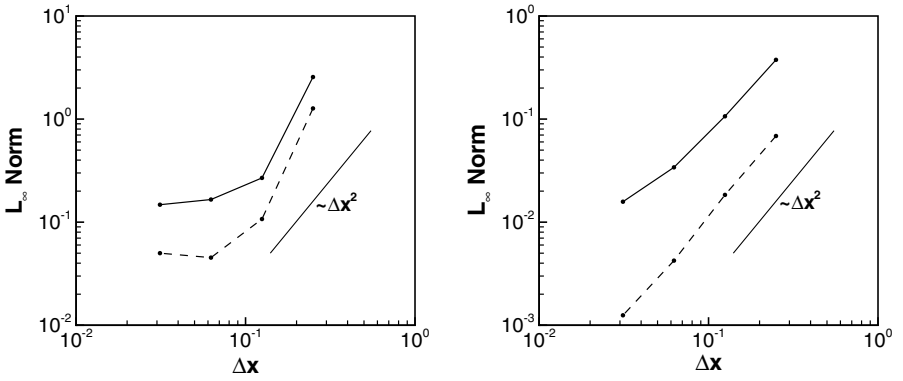

Fig. 2. L_∞ norm of the error versus grid spacing for Shear Layer A (left) and B at $t = 20$. Solid lines correspond to the error norm of the streamwise velocity perturbation, u', and dashed to the transverse, v'. The error for Shear Layer A tends to a constant as grid spacing decreases due to a mismatch in the growth rate with the linear stability analysis prediction. Perturbations in Case B grow at the expected rate and the error converges at second-order rate.

spacing becomes smaller and all wavenumbers become sufficiently resolved, this type of error decreases rapidly. The analysis based on the correlation metric that follows shows that the perturbations in Case A grow at different rate than the one predicted from LSA. Even though the mismatch in the growth rate is quite small it is sufficient to destroy the convergence of the norms.

The observed different error norm behavior between the two cases cannot be attributed to code error since the identical code produces perfectly converging results for Case B. Quite likely, boundary condition implementation limitations leave an imprint on the solution that cannot be removed by mesh refinement alone. This hypothesis is consistent with the change in the type of characteristic boundary conditions from Case A to B, i.e., different number of characteristics specified at the boundary: subsonic (A) to supersonic (B). Since the local boundary treatment is based on one-dimensional projection methods, there is always possibility that waves transverse to the boundary remain close to it and that may contribute to a local contamination of the solution.

4.3. Correlation metrics

The r_1 correlation was evaluated for both test cases for values of the three-dimensional parameter space α_r, α_i, and x_0. If the computed solution is identical with that from LSA, r_1 has a global maximum in a period of x_0 with a value of unity. In reality, the computed solution will be close to the analytical solution, but will not be identical. Thus a maximum of the correlation is sought and this yields the values of α_r, α_i, and x_0 at the maximum. Their values should be close to the exact values used to force the shear layer. Since this is an unsteady flow, the correlation is computed at various times. Its maximum value and the values $(\alpha_r, \alpha_i, x_0)$ at the maximum will actually vary with time. In this study, the correlation maximum was always found to be near the value of the most-unstable mode with which the shear layer was forced and the correlation maximum was very close to unity.

Figs. 3 and 4 show results based on correlation r_1 for the streamwise velocity perturbation, u', and transverse velocity, v', at various grid spacings and times. The results can be seen to converge as the grid is refined with the value of the maximum of the correlation approaching unity, an indication that the shape of the perturbation field is the one predicted from the LSA.

Even though the correlation maximum is very close to unity for both cases, only in Case B does the growth rate converge to the value predicted by LSA. Perturbations in Shear Layer A appear to be growing at a slightly lower rate than expected. The discrepancy in the growth rate is about 1%.

Also shown in Figs. 3 and 4 is the real part of the mode which appears to converge to the correct result. Tables 4 and 5 show results at a resolution of 1600×640 ($\Delta x = 0.0625$) at time $t = 20$.

As a way of visualizing the relationship between the computed and LSA perturbation fields, scatter plots of the computed u' and v' versus the LSA values are shown in Figs. 5 and 6 for $\Delta x = 0.0625$ and $t = 20$. Each

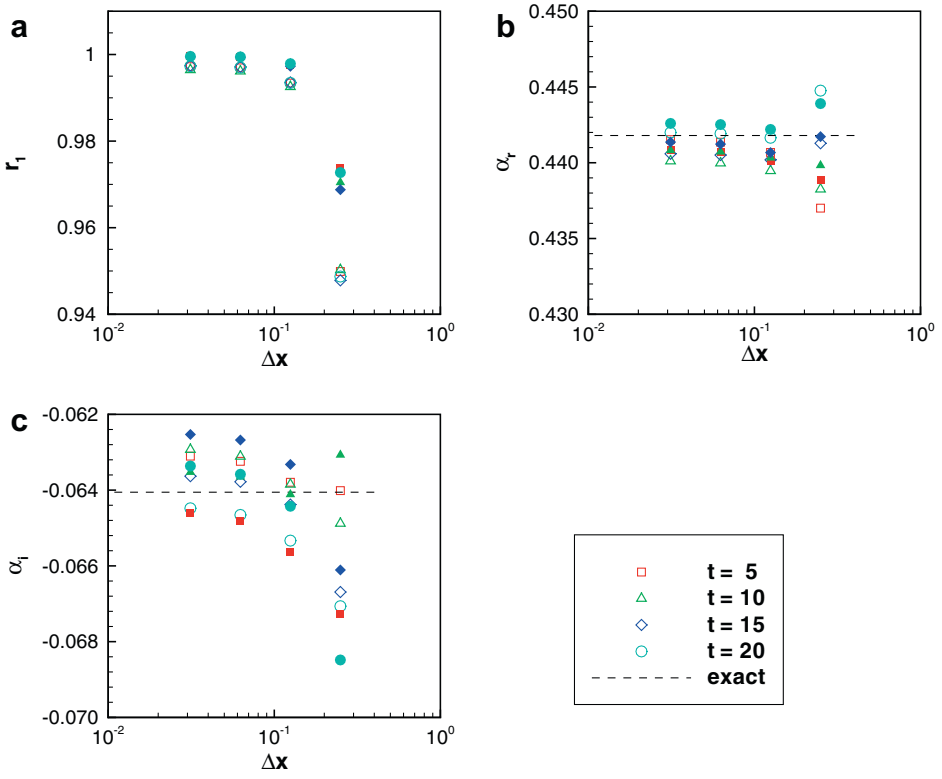

Fig. 3. Results for Shear Layer A at different times and resolutions. Correlation r_1 (a), the real part of the mode (b) and the imaginary part of the mode (c). Open symbols correspond to correlation with u' and filled symbols with v'.

point $(u'_{\mathrm{LSA},ij}, u'_{\mathrm{comp},ij})$ on the scatter plots represents the value of u' in the computational cell (x_i, y_j), $u'_{\mathrm{comp},ij}$, and the LSA value, $u'_{\mathrm{LSA},ij}$, at the same location and time. A closer look of Fig. 6 reveals that the computed solution for Case B grows slightly faster than the LSA predicted growth rate in accord with the results of Table 5.

The second type of correlation defined, r_2, is an implicit function of the disturbance frequency ω, in other words, this is a correlation along the dispersion relation. The eigenfunctions in this case are different for each value of $\alpha = \alpha(\omega)$. Fig. 7 shows the values of the correlation r_2 as a function of the frequency for both shear layers at time $t = 20$ computed on a 1600×640 grid. As in the case of the r_1 correlation, the maximum occurs at the most unstable mode and the value of r_2 decreases significantly away from the most unstable mode.

4.4. Discussion

To address practical difficulties with classical error metrics in comparing "spiky" fields that evolve in space or time, correlation metrics can be used in the verification of fluid-dynamics solvers. Convergence of the error norm is only possible when the growth rate converges to the one predicted from LSA. If there is a mismatch, owing to accumulation of dispersion errors introduced naturally in the discretization of the governing equations and the treatment of boundary conditions, for example, classical error norms may not converge even if the numerical solver is correct. In one of the test cases considered here, Shear Layer A, the growth rate of the computed solution differs slightly from the one predicted from LSA and, as a result, the L_∞ norm does not converge within the resolution range explored. Using the correlation metric we were able to quantify the discrepancy in the growth rate. Correlation metrics assume only the "shape" of the solution and not the growth rate. Our results show that this assumption is valid since the maximum of the correlation was always very close to unity.

Correlation metrics differ from classical error metrics and cannot be used as the only test in the verification of a fluid dynamics solver. However, they provide a complement to classical error assessment tools in a

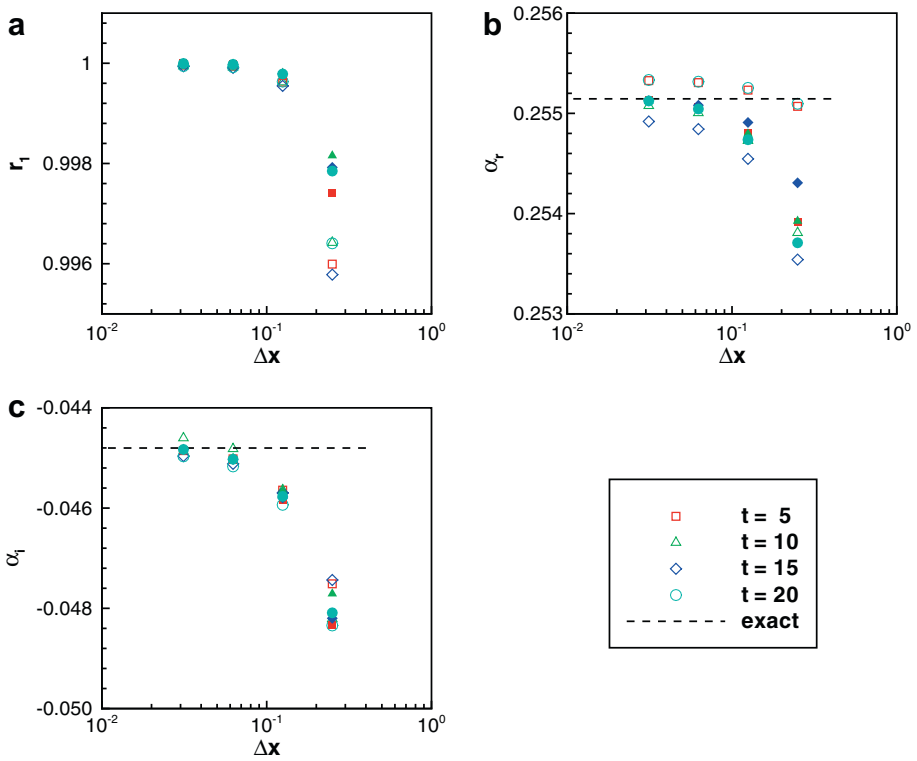

Fig. 4. Results for Shear Layer B at different times and resolutions. Correlation r_1 (a), the real part of the mode (b) and the imaginary part of the mode (c). Open symbols correspond to correlation with u' and filled symbols with v'.

Table 4
Comparison of the exact and computed real and imaginary parts of the most unstable mode for Shear Layer A for u' and v'. The grid resolution is 1600×640 ($\Delta x = 0.0625$)

Scaled time, t	Real part	Imaginary part	Correlation
Exact	0.441798	−0.064055	–
Correlation with u'			
5	0.441359	−0.063240	0.996917
10	0.439975	−0.063110	0.996149
15	0.440510	−0.063780	0.997158
20	0.441920	−0.064655	0.996986
Correlation with v'			
5	0.440709	−0.064812	0.999453
10	0.440722	−0.063648	0.999467
15	0.441230	−0.062678	0.999276
20	0.442520	−0.063581	0.999457

numerical-simulation verification program. A limitation of the correlation metric, as it is constructed here, is that the magnitude of the solution is not assessed because of the normalization of the correlation coefficient (Eq. (3)). Thus, an additional test is required.

While simple flows can be used to verify order-of-accuracy and convergence, the present technique utilizes results from LSA that provides solutions to the linearized partial differential equations of fluid flow so that a solver can be tested on a more complex problem with realistic boundary conditions. As is evident from the example of the spatial shear layer used in this study, boundary conditions are of particular significance. Perturbations are introduced at the inflow, convect downstream, and must exit at the outflow boundary without

Table 5
Comparison of the exact and computed real and imaginary parts of the most unstable mode for Shear Layer B for u' and v'. The grid resolution is 1600×640 ($\Delta x = 0.0625$)

Scaled time, t	Real part	Imaginary part	Correlation
Exact	0.255145	−0.044802	–
Correlation with u'			
5	0.255307	−0.045018	0.999941
10	0.255005	−0.044818	0.999922
15	0.254843	−0.045118	0.999908
20	0.255316	−0.045169	0.999922
Correlation with v'			
5	0.255064	−0.045047	0.999975
10	0.255055	−0.045001	0.999980
15	0.255081	−0.045030	0.999978
20	0.255044	−0.045026	0.999978

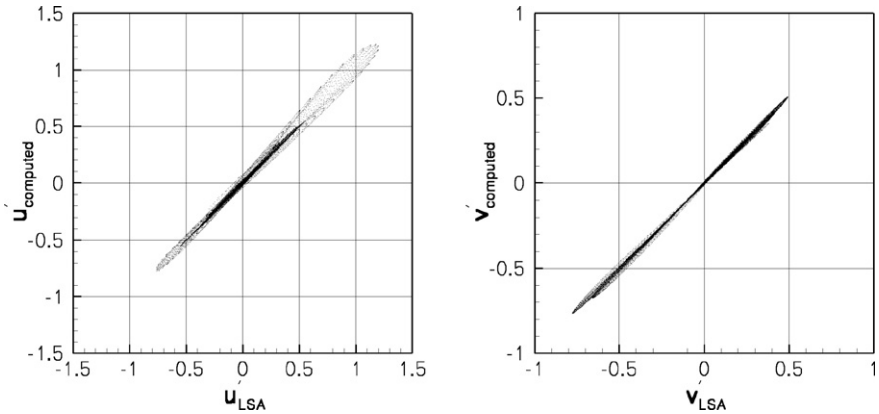

Fig. 5. Scatter plots for u' (left) and v' for Shear Layer A, $\Delta x = 0.0625$ and $t = 20$.

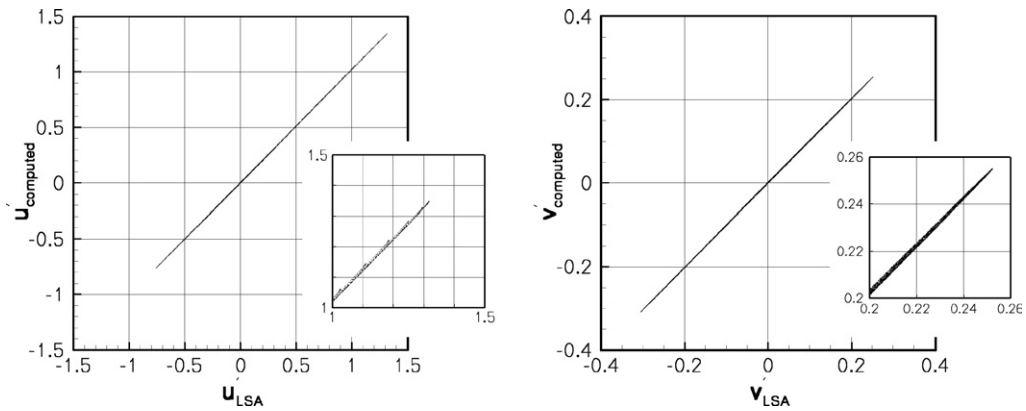

Fig. 6. Scatter plots for u' (left) and v' for Shear Layer B, $\Delta x = 0.0625$ and $t = 20$.

excessively contaminating the flow with spurious reflections. Failure to impose the correct inflow condition or the presence of spurious reflected waves at outflow boundaries will cause a reduction in the correlation and a deviation of the growth rate from LSA predictions. For this reason, while the methodology described here verifies the solver, it is particularly valuable in that it also verifies the particular boundary closure.

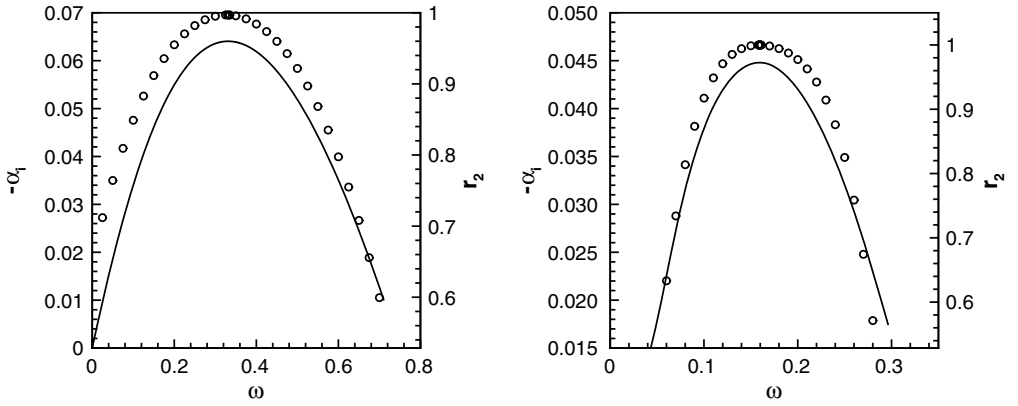

Fig. 7. Correlation r_2 (circles) as a function of the frequency ω for Shear Layer A (left) and B at time $t = 20$. Also plotted is the dispersion relation (continuous line). This tests the value of ω where the maximum occurs, which can be seen to be in excellent agreement with the LSA values.

Furthermore, the current method does not require modification of the solver, as does the method of manufactured solutions, where additional/separate treatment for source terms is required, and can be used for the verification of "black-box" solvers where the user has no access to the source code.

Even though in the example of the instability of a spatial laminar shear layer presented here, a normal-mode methodology is used to derive the stability characteristics of the basic flow, the verification methodology is not restricted to normal linearized operators. If the linearized equations about a basic flow exhibit non-normal behavior and therefore transient growth [8], a modified technique from that presented here may be required. The main idea is to compare a solution of the linearized equations to a solution from a non-linear solver using a projection-based method. In many cases, the linearized problem reduces to the solution of an ordinary differential equation for which solution methods are well developed and can be readily verified. This feature of the use of LSA solutions makes them attractive for verification of non-linear multi-dimensional partial differential equations solvers. Care should be taken so that the conditions for the comparison are satisfied. For example, in the two shear layer cases examined here, the amplitude of the perturbations should be sufficiently small for the assumption of linearity (Eq. (14)) to be satisfied throughout the domain.

The proposed method can be extended to three dimensions and other flows for which LSA can be applied. Extending the example discussed here, one could consider oblique wave disturbances, for example, of the form,

$$Q'(x,y,z,t) = f(y)\exp[\mathrm{i}(\alpha x + \beta z - \omega t)]. \tag{17}$$

In this case, the parameter space of the correlation would be expanded to include the values of the spanwise component.

5. Conclusions

A method utilizing results from linear stability analysis (LSA) theory is used for computer source code verification of fluid-dynamics solvers including boundary conditions. We show through an example of compressible shear layers that the exponentially growing nature of the LSA solutions results in poor measurement of the convergence rate if classical error metrics are used, such as the p-norms of the error. An alternative approach based on the use of correlations is presented here by which the solution obtained from a numerical solver is correlated with the LSA solution. The comparison in terms of a correlation helps assess whether the perturbations evolve correctly and grow at the expected rate. Numerical solutions for an unbounded (effectively) incompressible shear layer and a confined compressible shear layer are computed using a compressible flow solver to demonstrate how the present method can be applied to the verification of the numerical solution of Euler flows.

Acknowledgments

This work was supported by AFOSR Grants FA9550-04-1-0020 and FA9550-04-1-0389, by the Caltech DOE Advanced Simulation and Computing (ASC) Alliance Center under subcontract No. B341492 of DOE contract W-7405-ENG-48, and NSF Grant EIA-0079871. We would like to acknowledge Ralph Deiterding and David Hill for their contributions to and support of the AMROC framework, and Dan Meiron and Dale Pullin for discussions. We would like to thank the Center for Advanced Computing Research at Caltech and the Livermore Computing Center at Lawrence Livermore National Laboratory for technical assistance.

References

[1] W. Blumen, Shear layer instability of an inviscid compressible fluid, J. Fluid Mech. 40 (1970) 769–781.
[2] W. Blumen, P.G. Drazin, D.F. Billings, Shear layer instability of an inviscid compressible fluid. Part 2, J. Fluid Mech. 71 (1975) 305–316.
[3] A.W. Cook, P.E. Dimotakis, Transition stages of Rayleigh–Taylor instability between miscible fluids, J. Fluid Mech. 443 (2001) 69–99.
[4] R. Deiterding, Parallel adaptive simulation of multi-dimensional detonation structures, Ph.D. Thesis, Techn. Univ. Cottbus, September 2003.
[5] R. Deiterding, AMROC – Blockstructured Adaptive Mesh Refinement in Object-oriented C++, <http://amroc.sourceforge.net>, October 2004.
[6] P.G. Drazin, A. Davey, Shear layer instability of an inviscid compressible fluid. Part 3, J. Fluid Mech. 82 (1977) 255–260.
[7] S. Goldberg, Probability: An Introduction, Prentice-Hall, Inc., Englewood Cliffs, NJ, 1960.
[8] G. Han, A. Tumin, I. Wygnanski, Laminar-turbulent transition in Poiseuille pipe flow subjected to periodic perturbation emanating from the wall. Part 2. Late stage of transition, J. Fluid Mech. 419 (2000) 1–27.
[9] L. Hatton, The T experiments: errors in scientific software, IEEE Comput. Sci. Eng. 4 (2) (1997) 27–38.
[10] D.J. Hill, D.I. Pullin, Hybrid tuned center-difference-WENO method for large eddy simulations in the presence of strong shocks, J. Comput. Phys. 194 (2) (2004) 435–450.
[11] A.E. Honein, P. Moin, Higher entropy conservation and numerical stability of compressible turbulence simulations, J. Comput. Phys. 201 (2) (2004) 531–545.
[12] L. Kaiktsis, P.A. Monkewitz, Global destabilization of flow over a backward-facing step, Phys. Fluids 15 (12) (2003) 3647–3658.
[13] P. Knupp, K. Salari, Verification of Computer Codes in Computational Science and Engineering, Chapman and Hall/CRC, Boca Raton, FL, 2003.
[14] M. Lessen, J.A. Fox, H.M. Zien, On the inviscid stability of the laminar mixing of two parallel stream of a compressible fluid, J. Fluid Mech. 23 (1965) 355–367.
[15] M. Lessen, J.A. Fox, H.M. Zien, Stability of the laminar mixing of two parallel streams with respect to supersonic disturbances, J. Fluid Mech. 25 (1966) 737–742.
[16] R.P. McDonald, Factor Analysis and Related Methods, Lawrence Erlbaum Associates, Hillside, NJ, 1985.
[17] R.W. Metcalfe, S.A. Orszag, M.E. Brachet, S. Menon, J.J. Riley, Secondary instability of a temporally growing mixing layer, J. Fluid Mech. 184 (1987) 207–243.
[18] A. Michalke, On the inviscid instability of the hyperbolic-tangent velocity profile, J. Fluid Mech. 19 (4) (1964) 543–556.
[19] W.L. Oberkampf, T.G. Trucano, Verification and validation in computational fluid dynamics, Prog Aerosp. Sci. 38 (3) (2002) 209–272.
[20] C. Pantano, R. Deiterding, D.J. Hill, D.I. Pullin, A low-numerical dissipation patch-based adaptive mesh refinement method for large-eddy simulation of compressible flows, J. Comput. Phys. 221 (1) (2007) 63–87.
[21] D. Papamoschou, A. Roshko, The compressible turbulent shear layer: an experimental study, J. Fluid Mech. 197 (1988) 453–477.
[22] D. Partridge, A New Guide to Artificial Intelligence, Ablex Publishing Corp., Norwood, NJ, 1991.
[23] T.J. Poinsot, S.K. Lele, Boundary-conditions for direct simulations of compressible viscous flows, J. Comput. Phys. 101 (1) (1992) 104–129.
[24] M.J.D. Powell, Approximation Theory and Methods, Cambridge University Press, Cambridge, UK, 1981.
[25] S. Ravier, M. Abid, M. Amielh, F. Anselmet, Direct numerical simulations of variable-density plane jets, J. Fluid Mech. 546 (2006) 153–191.
[26] P.J. Roache, Verification and Validation in Computational Science and Engineering, Hermosa Publishers, New Mexico, 1988.
[27] C.J. Roy, Review of code and solution verification procedures for computational simulation, J. Comput. Phys. 205 (1) (2005) 131–156.
[28] S. Steinberg, P.J. Roache, Symbolic manipulation and computational fluid dynamics, J. Comput. Phys. 57 (2) (1985) 251–284.
[29] B. Strand, Summation by parts for finite-difference approximations for d/dx, J. Comput. Phys. 110 (1) (1994) 47–67.
[30] K.W. Thompson, Time dependent boundary conditions for hyperbolic systems, J. Comput. Phys. 68 (1987) 1–24.
[31] M. Zhuang, P.E. Dimotakis, T. Kubota, The effect of walls on a spatially growing supersonic shear layer, Phys. Fluids A 2 (4) (1990) 599–604.
[32] M. Zhuang, T. Kubota, P.E. Dimotakis, Instability of inviscid, compressible free shear layers, AIAA J. 28 (10) (1990) 1728–1733.